Proton Transfers in the Photochemical Reaction Cycle of Proteorhodopsin[†]

Andrei K. Dioumaev,[‡] Leonid S. Brown,[‡] Jennifer Shih,[‡] Elena N. Spudich,[§] John L. Spudich,[§] and Janos K. Lanyi*,[‡]

Department of Physiology & Biophysics, University of California, Irvine, California 92697 and Department of Microbiology & Molecular Genetics and Structural Biology Center, The University of Texas Medical School, Houston, Texas 77030

Received January 18, 2002; Revised Manuscript Received February 28, 2002

ABSTRACT: The spectral and photochemical properties of proteorhodopsin (PR) were determined to compare its proton transport steps to those of bacteriorhodopsin (BR). Static and time-resolved measurements on wild-type PR and several mutants were done in the visible and infrared (FTIR and FT-Raman). Assignment of the observed C═O stretch bands indicated that Asp-97 and Glu-108 serve as the proton acceptor and donor, respectively, to the retinal Schiff base, as do the residues at corresponding positions in BR, but there are numerous spectral and kinetic differences between the two proteins. There is no detectable dark-adaptation in PR, and the chromophore contains nearly entirely all-*trans* retinal. Because the pK_a of Asp-97 is relatively high (7.1), the proton-transporting photocycle is produced only at alkaline pH. It contains at least seven transient states with decay times in the range from 10 μs to 200 ms, but the analysis reveals only three distinct spectral forms. The first is a red-shifted K-like state. Proton release does not occur during the very slow (several milliseconds) rise of the second, M-like, intermediate, consistent with lack of the residues facilitating extracellular proton release in BR. Proton uptake from the bulk, presumably on the cytoplasmic side, takes place prior to release ($\tau \sim 2$ ms), and coincident with reprotonation of the retinal Schiff base. The intermediate produced by this process contains 13-*cis* retinal as does the N state of BR, but its absorption maximum is red-shifted relative to PR (like the O state of BR). The decay of this N-like state is coupled to reisomerization of the retinal to all-*trans*, and produces a state that is O-like in its C−C stretch bands, but has an absorption maximum apparently close to that of unphotolyzed PR.

Type I rhodopsins are photoactive seven-helical membrane proteins that covalently bind all-*trans* retinal via a lysine-Schiff base at helix 7 (*1*). There is substantial conservation of residues in the retinal-binding pocket, and these proteins are homologous to the haloarchaeal rhodopsins but not to the visual rhodopsins of higher eucaryotes (type II). Until a few years ago, this family consisted of four groups of proteins found only in haloarchaea: the two ion pumps bacteriorhodopsin (BR[1]) and halorhodopsin, and the two photoreceptors sensory rhodopsin I and sensory rhodopsin II. Genome sequencing projects have led to the discovery of many additional members from eubacterial and eucaryotic as well as archaeal organisms. Proteins most similar to BR and sensory rhodopsin II were found in lower eucaryotes, such as *Neurospora* and other ascomycetes (*2*, *3*). Although the residues necessary for proton pumping in BR are conserved, heterologously expressed rhodopsin from *Neurospora crassa* showed no proton transport, and its photochemistry was more similar to that of sensory rhodopsin II (*2*, *4*). These eucaryotic microbial rhodopsins may have photosensory functions, but their signaling cascades are as yet unknown.

The discovery of a BR-like protein in the uncultivated marine γ-proteobacterium of the SAR86 group (*5*) expanded the family of type I rhodopsins to include representatives of Eubacteria. Several variants of this protein, spectrally tuned to the light quality of the habitat of their hosts, were reported recently (*6*). When expressed in *Escherichia coli*, this protein (called proteorhodopsin, or PR) bound retinal to form a pigment that absorbed in the visible range, had a relatively rapid photoreaction cycle characteristic of transport rather than slow-cycling sensory rhodopsins, and showed substantial proton transport activity both in cells and right-side-out membrane vesicles (*5*). The initial characterization of the PR photocycle revealed at least two distinct intermediates, with spectra like those of the M and O states of BR (*5*). Later, the protein was shown to possess the same photochemistry in its native proteobacterial membranes, and from its flash-induced absorbance changes it was estimated to be a major membrane protein of its host (*6*). From these findings, and the conservation of many intramembrane residues important for proton transport in BR, it was concluded that PR is a light-driven proton pump in marine picoplankton (*5*, *6*).

We have investigated the pathway of the proton translocation in PR and compared it to that in BR. Asp-97 and Glu-108 in PR are homologues of the two most important proton

[†] This work was supported partly by National Institutes of Health Grants GM29498 (to J.K.L.) and GM27750 (to J.L.S.), Department of Energy Grant DEFG03-86ER13525 (to J.K.L.), and a Robert A. Welch Foundation award (J.L.S.).

* To whom correspondence should be addressed. Phone: (949) 824-7150. Fax: (949) 824-8540. E-mail: jlanyi@orion.oac.uci.edu.

[‡] University of California.

[§] The University of Texas Medical School.

[1] Abbreviations: BR, bacteriorhodopsin; PR, proteorhodopsin; K, L, M, N and O, intermediates of the photocycle; DM, *n*-dodecyl β-D-maltoside; CAPSO, 3-(cyclohexylamino)-2-hydroxy-1-propanesulfonic acid; FWHM, full width at half maximum; FTIR, Fourier transform infrared.

10.1021/bi025563x CCC: $22.00
Published on Web 04/09/2002

acceptors/donors of BR, Asp-85 and Asp-96. Experiments with *Neurospora* rhodopsin (*4*) had indicated, however, that the presence of carboxylic residues corresponding to Asp-85 and Asp-96 of BR are guarantees of neither proton transport nor reprotonation of the Schiff base by the Asp-96 homologue. Thus, to determine the proton pathway of PR it was necessary to examine closely the photocycles of the wild-type PR and mutants at these key positions. The Glu-108/Ser-65 pair in PR, corresponding to the Asp-96/Thr-46 pair of BR, is a conservative difference, but there are several other differences that are more likely to affect proton translocation. The two essential glutamic acids in the extracellular proton-release complex in BR, Glu-194 and Glu-204 (*7*, *8*), are not protonatable residues in PR, and the F−G loop, where they are located, contains mostly hydrophobic residues. If proton release occurs in the PR photocycle upon deprotonation of the Schiff base, it would have to be based on a different mechanism than in BR.

In this paper, we describe the pathway of proton translocation in the photochemical reaction cycle of PR expressed in *E. coli*. We characterized wild-type and mutant PR by time-resolved and static spectroscopy in the infrared and visible ranges. We replaced Asp-97 and Glu-108 with nonprotonatable residues, and searched for changes in the photocycle characteristic for removal of the key proton donors/acceptors. We also employed Asp/Glu and Glu/Asp replacements of these residues to assign their infrared bands. Analysis of these spectroscopic data shows that despite differences in primary structures, the major steps of the proton translocation are similar in the two proteins. On the other hand, the photocycle kinetics and the spectra of the intermediates show interesting differences that will need to be explained in molecular terms.

MATERIALS AND METHODS

Wild-type (C-terminally 6xHis-tagged) PR was expressed in *E. coli* (strain UT5600) as described before (*5*). Plasmids encoding the D97N, D97E, and E108Q mutants were constructed by a two-step PCR mutagenesis by a modification of the megaprimer method (*9*) using as template the pBAD TOPO plasmid containing the wild-type gene described previously (*5*). The E108D mutant was generated from a wild-type PR cDNA clone plasmid using the QuikChange Site-Directed Mutagenesis kit (Stratagene). The mutagenic oligonucleotides 5′-CCTCTATTAATATGT-GATTTCTACTTGATTCTTGCTGC-3′ and 5′-GCAGCAA-GAATCAAGTAGAAATCACATATTAATAGAGG-3′ were designed to introduce the E108D substitution, which resulted in the loss of a recognition site for the restriction enzyme EcoRI. A silent mutation at Leu-111 (underlined) was also introduced to avoid star activity of EcoRI for prescreening purpose. The D97E/E108Q double mutant was made by digestion of plasmids containing D97E and E108Q substitutions with restriction enzyme AseI. The 1.6 kilobase (kb) AseI fragment containing the E108Q substitution was gel purified and then ligated to the 3.17 kb AseI fragment of the plasmid with the D97E substitution. The resultant 4.77-kb plasmid was transformed into XL1-Blue cells (Stratagene, La Jolla, CA) and screened for double mutants. Positive mutants were selected by restriction enzyme mapping and subsequently confirmed by DNA sequencing (performed at Laragen, Inc., Santa Monica, CA). The constructs were then introduced into *E. coli* outer membrane protease-deficient strain UT5600 (*10*) for protein expression. Expression was induced by L-arabinose (0.2%, w/v), and the cells were grown in the presence of 5 μM all-*trans*-retinal, as described (*5*).

Membranes containing wild-type or mutant PR were isolated by resuspending washed (with 100 mM NaCl) *E. coli* cells in about 1/10 culture volume of 100 mM NaCl with addition of 100 μg/mL lysozyme and DNAseI (Sigma). The suspension was stirred for 3−4 h to digest the cell walls. The cells were then broken using French press (Aminco) at 18 000 psi, and centrifuged at low speed (1000*g*) to remove unbroken cells. Alternatively, the cells were disrupted by sonication. The membranes were collected by centrifugation (39000*g*, 30 min), washed two times by centrifugation in distilled water (39000*g*, 30 min), and further purified on a sucrose step gradient (40 and 60%) overnight at 60000*g*. To obtain samples with lower turbidity, the membranes (either before or after the sucrose gradient) were treated with 0.2% DM for 30 min. The heavier fraction was discarded after centrifugation at 12000*g* for 10 min, and the supernatant was centrifuged at high speed (39000*g*, 30 min). The resulting pellet was washed once more, and resuspended in the desired buffer.

Samples for FTIR measurements were prepared by sedimenting the DM-treated membranes at 200000*g* for 1 h in the buffer of desired pH (9.2−10.0, 50 mM CHES or CAPSO in the presence of 150 mM NaCl). The pellet was squeezed between two CaF_2 windows using a 6 or 15 μm spacer (Spectra-Tech Inc., Shelton, CT); approximately 45% of the volume in these samples is liquid (*11*). At least two similarly but separately prepared samples were measured for each case. All measurements were done using a temperature controlled sample holder (Harrick, Ossining, NY), connected to a water bath (RTE−111, Neslab, Portsmouth, NH).

The FTIR time-resolved measurements were performed on a Bruker IFS-66s instrument, in the spectral range of 0−2000 cm^{-1} at 2 cm^{-1} resolution. Interferograms were collected in the rapid-scan mode with 85 ms time-resolution. Excitation was provided by the second harmonics of a Nd:YAG laser (Minilite II, Continuum, Santa Clara, CA) at 532 nm, with ∼7 ns pulse width, and ∼2 mJ/cm^2 pulse energy. The laser pulses were spaced at times greater than 5× the slowest decay time constant. Static FTIR spectra were measured as described before (*12*).

Kinetic analysis of optical data (in IR and visible ranges) was as described before (*11*, *13*, *14*). The data were simultaneously fitted at many wavelengths/wavenumbers with a sum of exponentials using the program FITEXP (*13*). The number of statistically valid kinetic components was calculated by comparing results from two methods: global (i.e., multiexponential) fitting and SVD. First, F-test statistics was applied to the multiexponential fits with (n) and (n + 1) components to find a threshold beyond which adding an extra exponential fails to improve the quality of the fit significantly. Then, the 2D data array was subjected to SVD treatment in MATLAB, and "first correlation coefficients" were calculated for SVD-generated "kinetic components". As usual (*15*), correlation coefficients ≥0.6 were considered as evidence for systematic (i.e., nonrandom) contributions, and, therefore, the corresponding SVD components were retained as statistically valid.

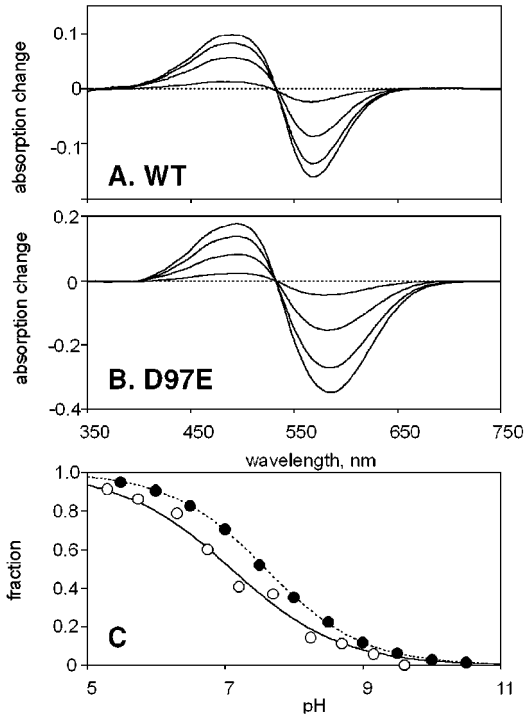

FIGURE 1: pH-dependence of the absorption spectrum of proteorhodopsin in polyacrylamide gel-encased, DM-treated membranes at 22 °C. (A) Difference spectra for wild-type membranes in 150 mM NaCl, 20 mM BTP, 3 mM MES and 3 mM succinate. The absolute spectrum at pH 5.3 was subtracted from spectra measured at pH 6.3, 7.2, 8.25, and 9.6 (in order of increasing amplitudes). (B) D97E membranes in 150 mM NaCl, 20 mM BTP, 20 mM CAPS, and 20 mM succinate. The absolute spectrum at pH 5.5 was subtracted from spectra at measured pH 6.5, 7.5, 8.5, and 10 (in order of increasing amplitudes). (C) Titration curves obtained from the data such as in A (open circles) and B (closed circles). The data were fitted with the Henderson−Hasselbalch equations, and yielded a pK_a = 7.1, n = 0.55 for the wild-type (open circles, solid line), and a pK_a = 7.6, n = 0.62 for D97E (closed circles, dotted line).

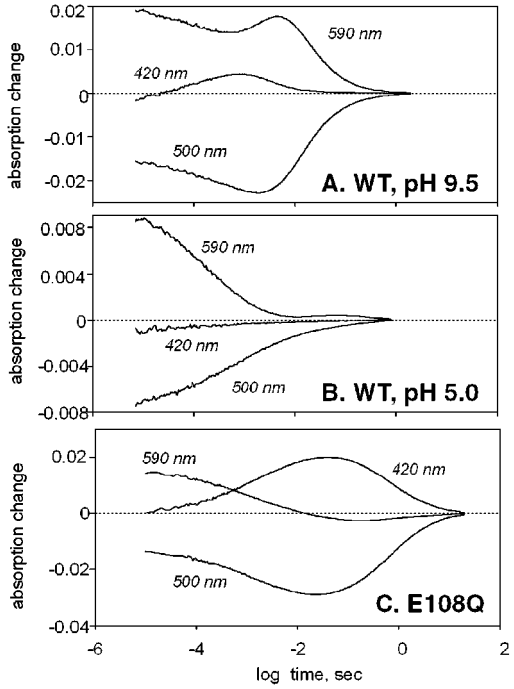

FIGURE 2: Time-courses of absorption changes of proteorhodopsin in polyacrylamide gel-encased, DM-treated membranes at 22 °C. Absorption changes after a laser pulse were followed at 420, 500, and 590 nm, and are shown on a logarithmic time-scale. (A) Wild-type membranes in 150 mM NaCl, 50 mM CAPSO, pH 9.5. (B) Wild-type membranes in 150 mM NaCl, 20 mM succinate, pH 5.0. (C) E108Q membranes in 150 mM NaCl, 50 mM CAPSO, pH 9.5.

Comparison of number of spectral components with the number of time-constants (see Results) suggested that nearly all transitions in the PR photocycle can be considered as reversible. If so, the observed time constants are not the true intrinsic rate constants of individual transitions but rather the apparent rates associated with observable transitions between transient equilibrium mixtures of intermediates. The spectra characterizing these transient mixtures were calculated with the program SCHEMEFIT. For more details on the FITEXP and the SCHEMEFIT programs, as well as on statistical tests on the number of valid components in kinetic analysis, see ref *13*.

FT-Raman measurements were performed as before (*4*), with a spectral resolution of 2 cm^{-1}. We used a concentrated suspension of PR membranes (OD > 10) and the Raman spectrum of the buffer was subtracted.

Static optical spectra were measured on a Shimadzu UV-1601 spectrophotometer. The kinetic measurements in the visible were as described earlier (*16*), using membranes encased in polyacrylamide gels or membrane suspensions. Sequential measurements of photocycle kinetics at 27 wavelengths led to gradual photodestruction of the sample (less than 20% at the end of the series). To correct for this, kinetic traces taken at different wavelengths were renormalized. Measurements of proton kinetics with pyranine (*17*) were performed in unbuffered membrane suspensions as before (*7*), but at low ionic strength (few mM of NaCl) to avoid membrane aggregation.

RESULTS AND DISCUSSION

pH-Dependent Equilibria in Wild-Type and Mutant Proteorhodopsins. In the pH range 4−11, wild-type PR exists in two distinct spectral forms, with absorption maxima at 520 (high pH) and 543 nm (low pH). Spectroscopic titration (Figure 1A) yields a protonation curve with a pK_a of 7.1 (Figure 1C). Because the photocycle of the low pH form (Figure 2B) lacks the M-like intermediate characteristic of the high pH form (Figure 2A, see also the detailed description of the photocycle below), it seemed likely that the titrated group is Asp-97, the homologue of Asp-85 that is the primary proton acceptor of the Schiff base of BR (*18*−*20*). This idea was confirmed by spectroscopic titration of the D97N PR mutant (not shown), which exists as a single spectral form between pH 5 and 9, with absorption maximum at 542 nm. Thus, the spectrum of the low pH PR species is almost identical to that of D97N mutant, similar to what was observed for BR (*21*). As in the BR mutant D85N (*22*), the D97N mutation causes a decrease in the pK_a of the Schiff base. We estimate from spectroscopic titrations a pK_a of about 10.3 in D97N, while in the wild-type (and in D97E) PR there is no evidence for Schiff base deprotonation at pH values up to 11 (data not shown). The photocycle of the D97N mutant, measured at pH 8.5 (not shown), is very similar to that of the low pH form of wild-type PR (Figure 2B), confirming the idea that the group responsible for existence of the two spectral forms of PR is indeed Asp-97. Thus, PR exhibits a spectral transition similar to the well-

known "blue-to-purple" transition of BR (*23*), although in PR both spectral forms are significantly (50−60 nm) blue-shifted, the pH-dependent spectral shift is smaller (815 vs 1320 cm^{-1}, in PR and all-*trans* BR, respectively), and the pK_a of the transition is about 4.5 pH units higher.

Titration of the D97E mutant (Figure 1B) revealed a similar spectral transition, with absorption maxima at 514 nm (blue-shifted from the wild-type PR) and at 565 nm (significantly red-shifted from the analogous form of the wild-type PR). The same trends of spectral shifts were observed between wild-type and D85E BR. In the latter, the titration is markedly biphasic, and occurs at strongly elevated pH from that of the wild-type BR (*24*, *25*). The transition in the D97E mutant of PR has a single pK_a of 7.6 (Figure 1C), i.e., only 0.5 pH units higher than for the wild-type. The biphasic character of this titration in BR originates from the coupling of the protonation states of Asp-85 and Glu-204 (*26*) and is abolished by the E204Q mutation (*25*). The lack of a Glu-204 homologue in PR therefore may be responsible for the monophasic titration. In the photocycle of the high pH form of D97E measured at pH 10 (not shown), the apparent rate of formation of the M intermediate is more rapid (about 10×) than that of the wild-type PR (Figure 2A). An even greater difference was found between M rise in the D97E mutant made in a E108Q background (not shown), where the slower decay allows development of the full amplitude of the M state. Rapid M rise was observed earlier in the photocycle of the D85E mutant of BR (*27*).

To characterize the chromophores of the different spectral forms of the wild-type and mutant PRs, we measured their FT-Raman spectra. These contain mostly bands from the retinal, with the exception of the strong protein amide-I band at 1660 cm^{-1} (*28*), which usually masks the weak vibrational band of the Schiff base. Figure 3 shows FT-Raman spectra for the high pH and low pH forms of the wild-type and D97E PR, as well as the single spectral form of D97N. As is well-known for BR and other retinal-binding proteins (*29*), the positions of the main ethylenic stretch bands of the retinal (1525−1537 cm^{-1}) are inversely proportional to their absorption maxima in the visible (514−565 nm). However, despite the presence of a distinct 1185 cm^{-1} band in the fingerprint region of each spectrum, which suggests that some amount of 13-*cis* isomer is present (*30*), we do not observe the corresponding shoulders in the main ethylenic stretch bands. Nor is the strong 800 cm^{-1} band typical for 13-*cis*-15-*syn* retinal in dark-adapted BR evident in these spectra. This means that in PR either the spectra of the 13-*cis* species are not shifted from the all-*trans* species, or more likely, their concentration is small. The fingerprint region is dominated by the C−C stretch bands characteristic for the all-*trans* retinal species (*31*). One band is located at around 1198 cm^{-1}, and has a pronounced satellite band (or shoulder) at 1208 cm^{-1} in D97N and low pH form of D97E (Figure 3, spectra c,d). Another conspicuous pair is located at 1163/1172 cm^{-1}, the 1163 cm^{-1} band being dominant in the species with negatively charged carboxylate at position 97 (Figure 3, spectra b,e), and the 1172 cm^{-1} band in the species with protonated carboxylic acid or asparagine (Figure 3a,c,d). A similar enhancement of the 1168 cm^{-1} band is seen in the Raman and FTIR difference spectra of the O intermediate of the BR photocycle, which also contains an all-*trans* chromophore and a protonated (uncharged) Schiff base

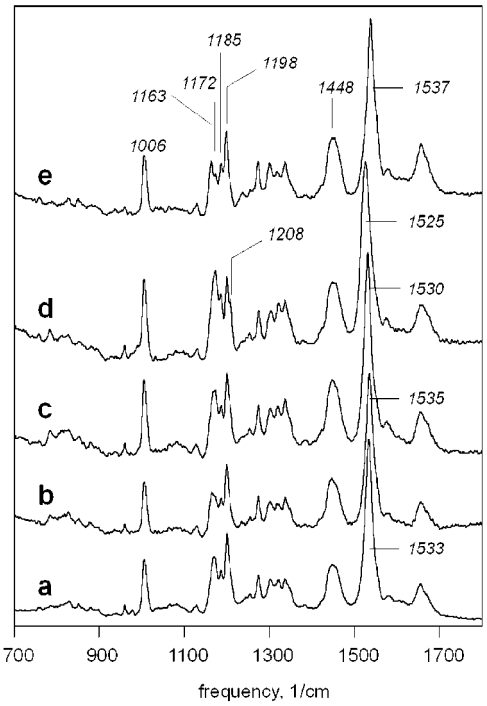

FIGURE 3: FT-Raman spectra of proteorhodopsin membrane suspensions (contribution of a buffer is subtracted). (a) Wild-type membranes in 100 mM NaCl, 50 mM BTP, 50 mM MES, pH 5. (b) Wild-type membranes in 50 mM Tris·HCl, 5 mM $MgCl_2$, pH 8. (c) D97N membranes in 50 mM Tris·HCl, 5 mM $MgCl_2$, pH 8. (d) D97E membranes in 50 mM Tris·HCl, 5 mM $MgCl_2$, pH 6.5. (e) D97E membranes in 100 mM CAPS, 5 mM $MgCl_2$, pH 10.

counterion (*32*−*34*). The 1006 cm^{-1} band of the methyl rock is downshifted about 4 cm^{-1} from the analogous band of BR, while the 1448 cm^{-1} band has unusually large amplitude. This band is assigned to asymmetric deformations of methyl groups of the retinal (*31*), and we observed a similar enhancement of this band in *Neurospora* rhodopsin (*4*).

Attempts to produce a "dark-adapted state" yielded no detectable shift in the Raman spectrum that would have indicated a change of isomeric composition, in 24 h. Static FTIR spectra indicated that illumination did not change the ratio of all-*trans* and 13-*cis*,15-*syn* retinal isomers, as would be observed in BR (data not shown).

Photocycle of Proteorhodopsin, Studied by Time-Resolved Spectroscopy in the Visible. Photocycle kinetics of the high pH form of wild-type PR were measured at three characteristic wavelengths: 500 nm to detect disappearance/reappearance of the initial state, 420 nm for deprotonation/reprotonation of the Schiff base, and 590 nm to detect red-shifted intermediates. The kinetics, shown in Figure 2A, are consistent with the earlier findings of a blue-shifted intermediate and a red-shifted state that follows it (*5*), and reveal an earlier red-shifted intermediate as well, which we term "K-like". The large fractional concentration of the K-like intermediate that persists throughout the 10−100 μs time domain is not observed in the BR photocycle. It may originate from kinetic causes, i.e., either a greatly slowed rate of decay or a dramatic shift of the K ↔ L equilibrium toward K. Alternatively, the K and L states of PR might both be red-shifted. In contrast, the photocycle of the low pH form of PR contains no detectable accumulation of an M-like state (Figure 2B). This is similar to the photocycle of the blue form of BR at acid pH (*35*).

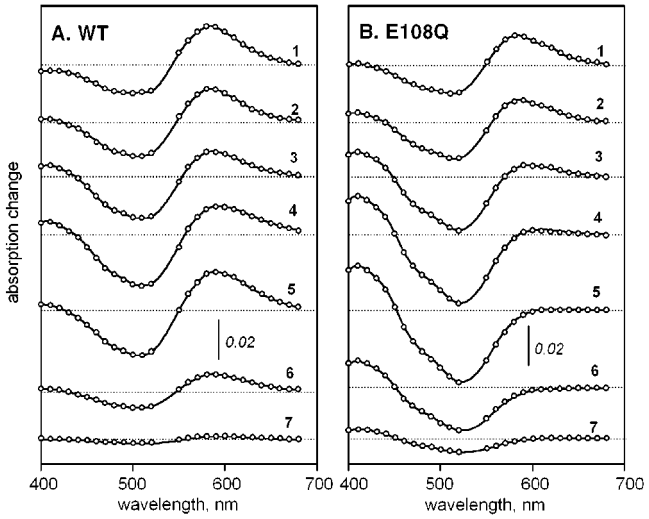

FIGURE 4: Apparent difference spectra (relative to the unilluminated sample) of mixtures of intermediates of the proteorhodopsin photocycle characterized by the time constants in Table 1. They were obtained by global seven-exponential fitting of data as in Figure 2, but at 27 different wavelengths. Circles represent the calculated points. The solid lines are cubic spline functions, included to guide the eye. Each spectrum (e.g., *n*th one) characterizes the mixture that would have been observed if one were able to block its decay (the *n*th kinetic component) while allowing all previous transitions (from the 1st up to the $(n-1)$th one) to be fully finished. These would correspond to the difference spectra of pure intermediates if (i) the cycle were unidirectional, and (ii) for each step the decay time constant were much slower than the correspondent rise time (i.e., $\tau_1 \ll \tau_2 \ll \tau_3 \ll \tau_4 \ll \tau_5 \ll \tau_6 \ll \tau_7$). Since neither of these two conditions hold, the plotted spectra are for mixtures of intermediates. (A) Wild-type, conditions as in Figure 2A. (B) E108Q mutant, conditions as in Figure 2C.

The decay rate of the late red-shifted intermediate is significantly slower in PR than in wild-type BR, but similar to the decay of the O state in BR mutants lacking Glu-194 and Glu-204 (*14*). This is to be expected, because the homologues of these residues are not protonatable in PR. However, the photocycle turn-over rate is far more rapid than in either the T90V or D115L mutants of BR (Dioumaev, Brown, Needleman, and Lanyi, unpublished results), indicating that the corresponding Val-102 and Ser-131 residues in PR have less perturbing influence than they would in BR. Another interesting feature of the PR photocycle is that the M-like intermediate is produced with very low amplitude, as measured at 420 nm (Figure 2A) or indeed at any wavelength above 400 nm (Figure 4A). The transient accumulation of M may be low because the reprotonation of the Schiff base is not much slower than its deprotonation, as for example in the V49A mutant of BR (*36*). In that mutant, a slower M decay upon replacing the Schiff base proton donor Asp-96 with Asn fully restored the M amplitude and revealed the true rate of its formation. Similarly, the E108Q mutant not only tests whether Glu-108 serves as a proton donor to the Schiff base, but also is useful to reveal the kinetics of the Schiff base deprotonation.

Photocycle kinetics for the E108Q mutant, at the same wavelengths as for the wild-type PR, are shown in Figure 2C. The M-like intermediate has a much larger amplitude than in wild-type PR, its decay is slowed more than 100-fold, and no late red-shifted state is observed. Indeed, the phenotype of the E108Q mutant is very similar to that of D96N BR (*27*, *37*), strongly suggesting that Glu-108 serves as a proton donor to the Schiff base. The similarity is extended to the pH-dependence of the decay rate of M in the E108Q mutant, and its marked acceleration by azide (data not shown), characteristics known for the D96N mutant of BR (*38*−*40*). Moreover, similar to D96N BR (*41*), the more rapid decay of M upon addition of azide allows accumulation of the red-shifted intermediate (not shown). As to the rise of the M state in PR, it is clear from the E108Q mutant that it is very slow and not complete before 10 ms (Figure 2C, see kinetic analysis below).

To understand the photocycles of PR and its E108Q mutant in greater detail, we performed multiexponential analysis of kinetic data recorded under the same conditions as in Figure 2, but at 27 wavelengths (every 10 nm between 400 and 680 nm, omitting 530 and 540 nm to avoid laser artifacts) in the time range of 10 μs to 2 s (20 s for the E108Q mutant). The data were fitted with 4, 5, 6, 7, or 8 exponentials. The risk factor in F-test statistics was near zero (<0.0005) for the increase from 5 to 6 and from 6 to 7 exponentials for both wild-type and E108Q data sets. The risk factors increased ~120× for the wild-type and ~200× for E108Q data sets when an eighth exponential was included, signaling that it is statistically invalid. Autocorrelation analysis of the kinetic components produced by SVD of the wild-type data resulted in correlation coefficients of 1.0, 0.98, 1.0, 0.87, 0.75, 0.70, and 0.57 for the first seven components, but 0.17 for the eighth component. For the E108Q data set, the autocorrelation analysis was restricted to the portion of the data after 0.7 ms. In this region, the correlation coefficients for the first seven components were 1.0, 1.0, 0.98, 0.97, 0.73, 0.53, and 0.52, while that of the eighth component was 0.19. The correlation coefficients for the sixth and the seventh SVD components of the E108Q data were near threshold values (above 0.5 but below 0.6) (*15*), making their statistical significance questionable. However, multiexponential refitting of kinetic components of SVD produced (in both data sets) the same time constants as direct fit of the experimental data, and an F-test-based analysis confirmed the validity of the seven-exponential approximation. The residual noise level for the seven-exponential approximation was 0.11×10^{-3} absorbance units for the wild-type and 0.13×10^{-3} absorbance units for the E108Q data. Therefore, we conclude that in both wild-type and E108Q seven distinct kinetic components are both needed and sufficient to account for all nonrandom variations in the data. This implies that seven distinct transient states were detected in both photocycles.

Table 1 presents the time constants from this analysis. The difference spectra of the mixtures of intermediates that are formed as transient equilibria in these apparent transitions are presented in Figure 4. Contributions from the low-pH form are negligible, as the pH was 2 pH units above the pK_a (cf. Figure 1). However, we cannot completely exclude components arising from the small amount of 13-*cis*,15-*syn* species in PR (cf. the FT-Raman data in Figure 3 and its discussion). In the wild-type data (Figure 4A), the first spectrum is dominated by the K-like state. The first two kinetic components ($\tau_1 \sim 12$ and $\tau_2 \sim 120$ μs) show the growth of an M-like state at the expense of the K-like species. Starting from the third process ($\tau_3 \sim 0.8$ ms) a second red-shifted state appears concomitant with continued growth of the M-like intermediate. Spectrally, this intermediate is O-like, but according to our FTIR data (see below) the retinal

Table 1: Apparent Time Constants of Multiexponential Global Fits of Data for the Photocycles of the Wild-Type PR and the E108D and E108Q Mutants[a]

	pH	temp °C	FTIR/VIS	τ_1, μs	τ_2, μs	τ_3, ms	τ_4, ms	τ_5, ms	τ_6, s	τ_7, s
WT	9.5	22	VIS/27λ	12 ± 3	120 ± 10	0.8 ± 0.1	2.1 ± 0.1	9.4 ± 0.5	0.035 ± 0.002	0.23 ± 0.04
WT	9.2	5	VIS/5λ						0.25 ± 0.08	1.5 ± 0.7
WT	9.2	5	FTIR						0.19 ± 0.02	1.2 ± 0.3
E108D	9.2	5	FTIR						0.19 ± 0.03	1.2 ± 0.2
E108Q	9.5	22	VIS/27λ	70 ± 20	550 ± 50	3.4 ± 0.3	23 ± 3	220 ± 30	0.80 ± 0.10	4.4 ± 0.3
E108Q	9.2	5	FTIR						1.70 ± 0.30	10 ± 2

[a] In the visible region, the data used for analysis were measured either at 27 or 5 wavelengths (marked as 27λ and 5λ), and the points before 10 μs were omitted due to laser artifact. For the FTIR measurements, the time resolution was 85 ms; the corresponding measurements in the visible (5 °C, second row) were analyzed in the time range > 100 ms.

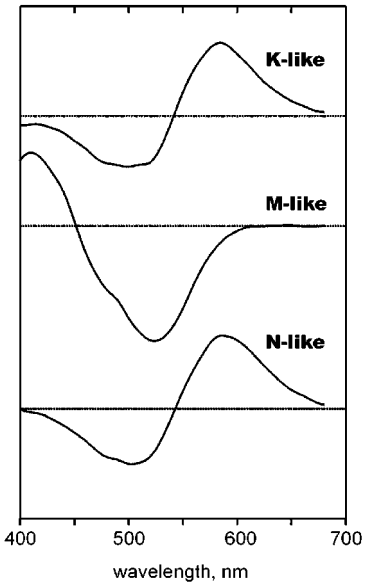

FIGURE 5: Calculated difference spectra for the K-like, the M-like, and the N-like intermediates. For K, spectrum 1, before the first decay component of the wild-type in Figure 4A is shown. For M, the average of spectra 5, 6, and 7 of the E108Q mutant in Figure 4B was taken. For N, spectrum 4 (with the greatest contribution from the M-like state) was subtracted interactively from the average of spectra 5, 6, and 7 of the wild-type in Figure 4A, until absorption around 400 nm was zero. The positive peaks in the spectra were scaled to be equal.

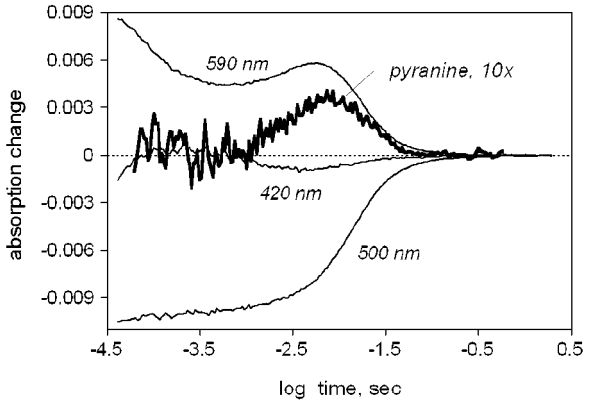

FIGURE 6: Kinetics of proton release and uptake by DM-treated proteorhodopsin membranes at 22 °C, pH 7.9. Absorption changes at 457 nm without pyranine were subtracted from those with pyranine (100 μM). Chromophore kinetics, obtained similarly to those in Figure 2, are shown for comparison.

is 13-*cis*, and therefore it appears to be a red-shifted N-like state, similar to one described earlier for Leu-93 mutants of BR (*33*, *42*). The major growth of the red-shifted, N-like state takes place during the τ_4 process (~2 ms), which is characterized by simultaneous disappearance of approximately half of the M-like state. The spectra corresponding to the last three kinetic components ($\tau_5 \sim 9.4$, $\tau_6 \sim 35$, and $\tau_7 \sim 230$ ms) could be scaled together (Figure 4A). The 3-exponential decay reflects disappearance of the red-shifted N-like-state in equilibrium with the earlier M-like state, with very small spectral changes.

As in the wild-type, the spectrum of the first kinetic component of the E108Q data set (Figure 4B) contains a K-like state with only minor contribution from the M-like species. The first four kinetic components ($\tau_1 \sim 0.07$, $\tau_2 \sim 0.55$, $\tau_3 \sim 3.4$, $\tau_4 \sim 23$ ms) reflect the four-exponential growth of an M-like state at the expense of the K-like intermediate. The last three components ($\tau_5 \sim 0.22$, $\tau_6 \sim 0.8$, and $\tau_7 \sim 4.4$ s) describe decay of the M-like state. Spectra of the M-state calculated for these kinetic components are not different from the spectra calculated for the rise of M in this mutant. No red-shifted intermediate is seen in E108Q, in accordance with similar data on the D96N mutant of BR (*43*).

Simple manipulation of the wild-type data produced three distinct difference spectra: a K-like, an M-like, and a late red-shifted N-like state. Likewise, the E108Q data set produced two spectra: a K-like, and an M-like. The best estimates for the difference spectra of the K-like, the M-like, and the N-like states are presented in Figure 5. It should be noted that no distinct contribution from an L-like state is immediately evident from our data. However, the multiexponential pattern of the K-to-M transition implies a presence of an L-like state between the K-like and the M-like states in the main path of the photocycle of PR. Failure to extract its spectrum by simple subtraction could be explained either with a spectral similarity to the K-like state, or with kinetics that hides its accumulation, as discussed above. Likewise, the kinetic data in the visible gave almost no clues about details of the later stages of the photocycle, and it was the FTIR data that produced the insights into these steps (see below).

Proton Kinetics in Proteorhodopsin. To detect proton release and uptake during the photocycle, we used the pH-sensitive dye pyranine (*17*). The results show (Figure 6) that proton uptake precedes proton release, the two processes being correlated with the rise and decay of the red-shifted N-like intermediate. This sequence is different from what is known for wild-type BR at physiological pH, but similar to the one observed for the E194Q and E204Q mutants of BR with a disabled proton-release complex (*8*, *14*). The main

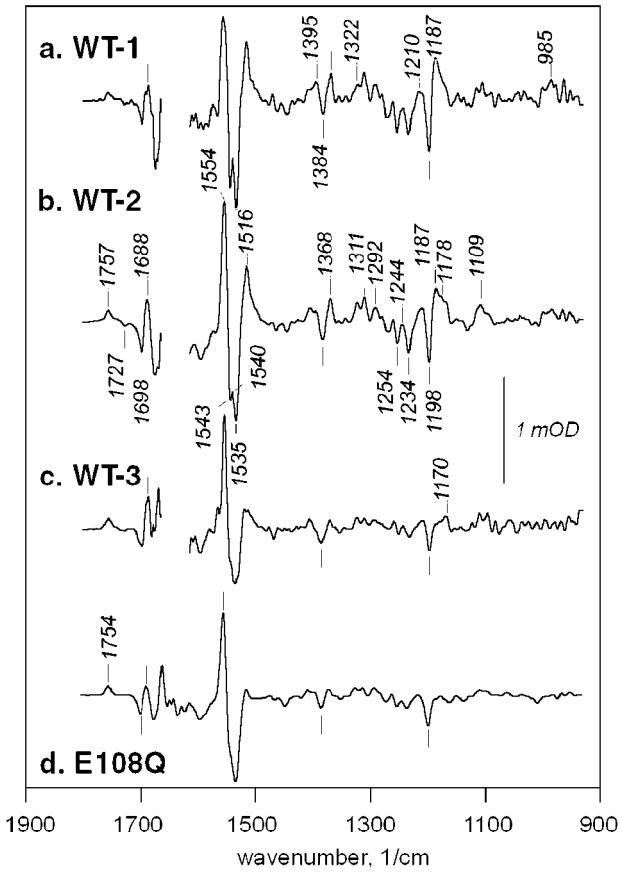

FIGURE 7: FTIR difference spectra of the wet PR membranes at 5 °C. (a) Wild-type, first measured spectrum; (b) Wild-type, early kinetic component (before τ_6); (c) Wild-type, late kinetic component (before τ_7); (d) E108Q mutant, last kinetic component, determined from a photostationary state (the spectra of the last decay components were nearly identical).

difference from BR is that in PR the retinal remains 13-*cis* after proton uptake and reprotonation of Glu-108, but in wild-type BR under physiological conditions reisomerization of the retinal to all-*trans* is coincident with uptake (*44*). In BR, the coupling of proton uptake and reprotonation of the proton donor, Asp-96, to reisomerization of the retinal is strong, although it can be broken by mutations of residues near the cytoplasmic surface (*12*). Evidently, analogous coupling is absent in wild-type PR.

Photocycle of Proteorhodopsin, Studied by Time-Resolved and Static FTIR Spectroscopy. Kinetic analysis allowed separation of the last two decay components ($\tau_6 \sim 190$ ms and $\tau_7 \sim 1.2$ s, at 5 °C), observed also in the visible region ($\tau_6 \sim 250$ ms and $\tau_7 \sim 1.5$ s, at 5 °C). Figure 7 shows spectra for the first time-slice of the rapid-scan measurement (spectrum a, within 85 ms of the flash), and the transient equilibria formed before the two apparent decay components (spectra b and c). The three spectra in Figure 7 (a, b, and c) show the familiar pattern of the fingerprint region of late intermediates of the photocycle of retinal proteins, i.e., bands at 1254, 1234, 1198, 1187, 1178, 1170 cm^{-1} (*4*, *34*, *45*, *46*). They differ both in shape (reflecting different mixtures of intermediates) and in absolute amplitude. For comparison, they were scaled at 1757 cm^{-1}, i.e., at the protonated carboxyl C═O band of Asp-97 (see the assignment below). Such scaling simultaneously normalized the spectra at 1109, 1170, 1384, and 1698 cm^{-1}, i.e., at the other prominent IR bands.

Similar to the D96N mutant of BR, E108Q of PR produces a photocycle with a long-living M (Figure 2), which can be accumulated under constant illumination. E108Q produced a typical M-like FTIR difference spectrum (Figure 7, spectrum d). As expected from other retinal proteins, this M-like spectrum is dominated in the 900−1500 cm^{-1} region by negative bands of the all-*trans* retinal, while positive contributions from 13-*cis* retinal are absent in the fingerprint region due to the deprotonated Schiff base (*47*, *48*).

The ethylenic stretch region in the M state (1505−1565 cm^{-1}) shows a depletion band at 1535 cm^{-1} (in accordance with the Raman data, cf. Figure 3), with a positive band at 1554 cm^{-1}; the latter may include a contribution from amide-II distortions (*49*). In the spectra from the wild-type protein (Figure 7, spectra a, b, and c), there is an additional positive band at 1516 cm^{-1}. The latter is evidence for a red-shifted intermediate (*32*), and is in accordance with the visible kinetic data. The change in the ratio of the 1516 and 1554 cm^{-1} bands from the early to the late spectra (Figure 7, spectra a, b, and c) indicates gradual disappearance of the red-shifted intermediate(s). The amount of M-like state expected from the data in the visible range in the τ_5, τ_6, and τ_7 spectra (cf. Figure 4) is not sufficient to account for the amplitude of the relative change at 1554 cm^{-1}. Therefore, a contribution from some other state, which is neither M-like nor red-shifted, should be present.

The negative ethylenic stretch band is structured (minima at 1535 and 1543 cm^{-1}, with cumulative FWHM ~21 cm^{-1} vs 13 cm^{-1} in BR), which originates probably from the overlap with a positive ethylenic stretch at 1540 cm^{-1}. The L and N states of BR are known to have double ethylenic stretch bands, at 1539/1551 and 1532/1549 cm^{-1} (*50*). In PR the double bands, at 1516 and 1540 cm^{-1}, may originate from an N-like state. Since we are dealing with mixtures, the decreased ratio of the 1516 and 1554 cm^{-1} bands must describe a shift, during the τ_6 process, from one mixture with a strong contribution of a red-shifted state to another with a stronger contribution of a not red-shifted species. This would be consistent with the conclusions from a different kind of kinetic analysis of the spectral changes in the visible (Váró, Brown, Lakatos, and Lanyi, manuscript in preparation).

What are the states in these mixtures? The spectra before the τ_6 process (Figure 7, spectra a and b) have several features that are considered to be the IR signature of the N state in the photocycle of BR. These are the strong and narrow ethylenic/amide-II band at 1554 cm^{-1}, the strong positive 1187 cm^{-1} band in the fingerprint region, the unusually strong (as compared with K, L, M, and O states) positive bands at 1395, 1368, and 1311 cm^{-1} (*51*). The strong positive bands at 1187, 1395, 1368, and 1311, but not the one at 1554 cm^{-1} disappear during the τ_6 process.

The most revealing changes take place in the fingerprint region. In Figure 7, spectrum a the 1187 cm^{-1} band is more prominent than the 1170 cm^{-1} band, but later in the cycle, in spectrum c, the positive bands at 1187 and 1178 cm^{-1} have nearly disappeared without effect on the 1170 cm^{-1} band. In retinal proteins, the positive band at 1187 cm^{-1} is from the 13-*cis* isomer (*30*), and in FTIR difference spectra it could be observed only in states with protonated Schiff

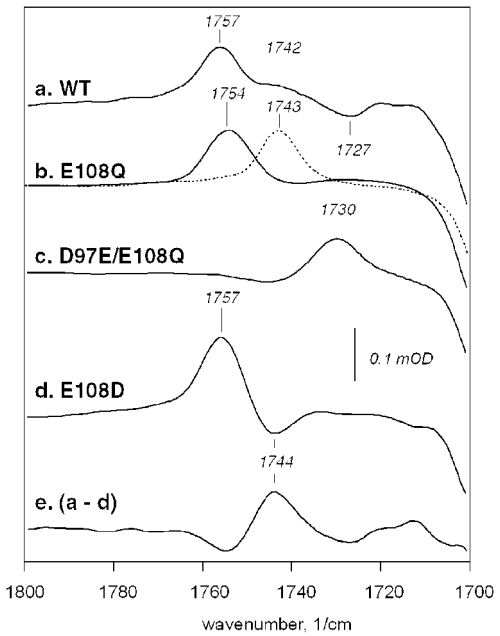

FIGURE 8: FTIR difference spectra as in Figure 7, but with the carboxylic stretch region expanded. (a) Wild-type; (b) E108Q mutant (dashed line measured in D_2O); (c) D97E/E108Q mutant (from photostationary state measurements); (d) E108D mutant; (e) result of subtracting spectrum d from spectrum a.

base (like L and N in BR (*34*)). On the other hand, the 1169 cm^{-1} band belongs to the all-*trans* retinal (*32*), and in FTIR difference spectra such positive bands appear only in species with a distorted all-*trans* chromophore, like the O state of BR (*34*, *45*). Thus, it appears that during the τ_6 process the mixture shifts from one containing predominantly a 13-*cis* isomer to another containing predominantly all-*trans*. In BR, such process would correspond to the N-to-O redistribution, and would be observed as an increase in contribution of red-shifted species. However, in PR the FTIR data show the opposite, a decrease in the contribution from a red-shifted state, while the visible data indicate hardly any change of the spectral shape (Figure 4). A possible explanation would be that the red-shifted N is in a mixture with an O state whose spectrum is similar to PR. Thus, decay of the unshifted O would not be detectable as a spectral change in the visible. If the spectrum of O is like the spectrum of the low pH species (the counterion to the Schiff base being protonated in both cases), this would be in accordance with the smaller spectral shift for the "purple to blue" transition in PR as compared to BR.

The changes in the carbonyl region above 1700 cm^{-1} during the photocycle are also very similar to those in BR. The absence of the homologue of Asp-115 of BR simplifies the spectral pattern, and during the late stages of the photocycle this region is dominated by three features: a positive peak at 1757 cm^{-1} with a strong shoulder around 1742 cm^{-1} and a negative peak at 1727 cm^{-1} (Figure 8, spectrum a). To reveal the origins of these peaks four mutants were prepared: E108D, E108Q, D97E, and D97E/E108Q.

Both the shoulder at 1742 cm^{-1} and the negative peak at 1727 cm^{-1} are absent in the M-like state of the E108Q (Figure 8, spectrum b), leaving a single peak at 1754 cm^{-1}. In N and O, i.e., the intermediates after M, this band is at 1757 cm^{-1} (Figure 7, spectra b and c, Figure 8, spectra a and d). This shift is the opposite to that in BR where the analogous band (from Asp-85) is at a lower frequency in the later intermediates than in M. The 1754 cm^{-1} peak is shifted to 1743 cm^{-1} upon H_2O to D_2O exchange (Figure 8, spectrum b, dashed line), confirming its assignment to a protonated carboxylic group. Upon Asp-to-Glu substitution in the double mutant D97E/E108Q, the 1754 cm^{-1} peak in the M-like state is downshifted to 1730 cm^{-1} (Figure 8, spectrum c). The 24 cm^{-1} downshift of the C═O band of the protonated Asp-97 upon its replacement with Glu is in the same direction, although smaller, than the 36 cm^{-1} downshift reported for the D85E mutation in BR (*18*, *20*) and the 41 cm^{-1} shift for the D73E mutant in sensory rhodopsin II (*46*). Therefore, the 1754 cm^{-1} band in M and the 1757 cm^{-1} band in N and O were assigned to the protonated Asp-97. Its protonated state in M suggests that it acts as the proton acceptor during Schiff base deprotonation. The same conclusion could be made from the spectrum of the D97E single mutant (not shown), but overlap of the downshifted positive 1730 cm^{-1} band of Glu-97 with the negative band at 1727 cm^{-1} of Glu-108 (see below) made the interpretation difficult. The 1757 cm^{-1} band of Asp-97 is present in the three last spectra (Figure 7, spectra a, b, and c) of the wild-type photocycle without any apparent shifts in either its position or shape. The negative 1384 cm^{-1} band, present in all three spectra to the same extent as the 1757 cm^{-1} band, is well suited for the symmetric carboxylate stretch frequency, and, therefore, at least part of its intensity is tentatively assigned to the symmetric C═O stretch of unprotonated Asp-97 in the unphotolyzed PR.

Unlike the Glu/Gln replacement in E108Q, neither the Glu/Asp exchange in E108D, nor the Asp/Glu exchange in D97E affect the photocycle strongly (not shown), and in the later part of the photocycle we observed the same mixtures of intermediates with only slightly changed ratios. The negative band of Glu-108 was assigned by comparing the FTIR spectra of the late intermediates in the wild-type and E108D photocycles. In E108D, the depletion band of Asp-108 was upshifted from 1727 to 1744 cm^{-1} (Figure 8, spectrum d). Again, this shift was smaller (17 cm^{-1}) than the corresponding shift (22 cm^{-1}) between the wild-type and the D96E mutant of BR (*52*). A negative C═O stretch band in this region, such as the 1744 cm^{-1} band, may originate from either deprotonation of a carboxylic acid or a frequency shift from environmental changes. When spectra a and d were scaled to minimize the difference in the 1000−1450 cm^{-1} region, the otherwise close match was disturbed at the positive Asp-97 band, which looked disproportionately stronger in the E108D mutant. Subtracting the trace for the E108D mutant from that of the wild-type (after this scaling) revealed (Figure 8, spectrum e) two negative bands (at 1727 and 1757 cm^{-1}) and one positive band (at 1744 cm^{-1}). That is, the protonated residue 108 is perturbed in the late intermediate (most probably N, which is the major species), which upshifts its C═O stretch band from 1727 to ∼1744 cm^{-1} when it is Glu and from 1744 to ∼1757 cm^{-1} when it is Asp. In the E108D mutant, the positive band from the latter shift overlaps with the band of Asp-97 at 1757 cm^{-1}. The results indicate, therefore, that Glu-108 is protonated in the red-shifted N state detected by FTIR, consistent with proton uptake earlier in the photocycle (Figure 6).

The perturbation of the reprotonated Glu-108 disappears during the τ_6 transition (Figure 7, spectrum c). Thus, Glu-108 is perturbed in N but not in the state that follows it. On the basis of the phenotype of the E108Q mutant, we concluded above that Glu-108 is the donor for Schiff base reprotonation. However, it is already reprotonated in the N state we detected, which, in turn, requires an existence of another N-like state (an earlier N) with deprotonated Glu-108, which should be formed in the time range prior to the starting point of our FTIR measurements. The frequency of the depleted C=O stretch band (1744 cm^{-1} for Asp-108) suggests that the pK_a of Asp-108 might be similar (>11) to that in BR. This pK_a increases further in the N state (as judged from the upshifted positive carboxylic band (*53*)), but will have reversed in the last intermediate.

CONCLUSIONS

The results indicate that proton transport by PR is based on a photochemical reaction cycle similar to, but not identical with, the photocycle of BR. Very approximately, the cycle may be described by the sequence PR $-h\nu \rightarrow$ K $\leftrightarrow$ (L?) $\leftrightarrow$ M $\leftrightarrow$ N $\leftrightarrow$ O (Váró, Brown, Lakatos, and Lanyi, manuscript in preparation), but the fact that the kinetics contain seven exponentials indicates that this is only an approximate scheme. The findings are summarized as follows:

(1) Unlike BR, which functions optimally between pH 4 and 8, PR has a photocycle consistent with proton transport only at pH > 7. The alkaliphilic character of PR is consistent with its marine origin since the pH of seawater is 7.6−8.2 (*54*). Whether Asp-97 is protonated or unprotonated, and whether the retinal isomers in the protein are allowed to come to thermal equilibrium, the chromophore of PR contains only minor amounts of 13-*cis*,15-*syn* retinal.

(2) The processes that precede deprotonation of the Schiff base include either a red-shifted L state or a K/L equilibrium strongly shifted toward K. The molecular basis for this is not clear. The differences between K and L in BR reside in both the retinal and the protein (*55*−*57*), and their functional significance will be perhaps better understood when these states are described in PR.

(3) Deprotonation of the Schiff base is kinetically complex, and not complete until tens of milliseconds. As a result, unless its decay is slowed by removing the proton donor Glu-108, the M state does not accumulate in amounts comparable to that of M of BR. The proton acceptor to the Schiff base is Asp-97, the homologue of Asp-85 in BR. A proton is not released during the rise of M, consistent with absence of the homologues of Glu-194 and Glu-204, i.e., a disabled extracellular proton release complex.

(4) Reprotonation of the Schiff base produces an intermediate analogous in its molecular properties to N, i.e., it contains a 13-*cis* retinal as well as protonated Schiff base and protonated Asp-97, but it has a red-shifted absorption maximum. Although the proton donor is Glu-108, the homologue of Asp-96 in BR, in the time-range resolved in the FTIR experiments we do not observe its unprotonated state. This is consistent with what is expected from the kinetics of proton uptake. If such an earlier N accumulates, it would be observed on the tens of millisecond time scale.

(5) Reisomerization of the retinal produces a state analogous to O, i.e., it contains a protonated Asp-97 as well as a perturbed all-*trans* retinal, but its absorption maximum appears to be not very different from that of unphotolyzed PR.

REFERENCES

1. Spudich, J. L., Yang, C. S., Jung, K. H., and Spudich, E. N. (2000) Retinylidene proteins: structures and functions from archaea to humans. *Annu. Rev. Cell Dev. Biol. 16*, 365−392.
2. Bieszke, J. A., Spudich, E. N., Scott, K. L., Borkovich, K. A., and Spudich, J. L. (1999) A eukaryotic protein, NOP-1, binds retinal to form an archaeal rhodopsin-like photochemically reactive pigment. *Biochemistry 38*, 14138−14145.
3. Idnurm, A., and Howlett, B. J. (2001) Characterization of an opsin gene from the ascomycete *Leptosphaeria maculans*. *Genome 44*, 167−171.
4. Brown, L. S., Dioumaev, A. K., Lanyi, J. K., Spudich, J. L., and Spudich, E. N. (2001) Photochemical reaction cycle and proton transfers in *Neurospora* rhodopsin. *J. Biol. Chem. 276*, 32495−32505.
5. Béjà, O., Aravind, L., Koonin, E. V., Suzuki, M. T., Hadd, A., Nguyen, L. P., Jovanovich, S. B., Gates, C. M., Feldman, R. A., Spudich, J. L., Spudich, E. N., and DeLong, E. F. (2000) Bacterial rhodopsin: evidence for a new type of phototrophy in the sea. *Science 289*, 1902−1906.
6. Béjà, O., Spudich, E. N., Spudich, J. L., Leclerc, M., and DeLong, E. F. (2001) Proteorhodopsin phototrophy in the ocean. *Nature 411*, 786−789.
7. Brown, L. S., Sasaki, J., Kandori, H., Maeda, A., Needleman, R., and Lanyi, J. K. (1995) Glutamic acid 204 is the terminal proton release group at the extracellular surface of bacteriorhodopsin. *J. Biol. Chem. 270*, 27122−27126.
8. Balashov, S. P., Imasheva, E. S., Ebrey, T. G., Chen, N., Menick, D. R., and Crouch, R. K. (1997) Glutamate-194 to cysteine mutation inhibits fast light-induced proton release in bacteriorhodopsin. *Biochemistry 36*, 8671−8676.
9. Chen, B., and Przybyla, A. E. (1994) An efficient site-directed mutagenesis method based on PCR. *Biotechniques 17*, 657−659.
10. Elish, M. E., Pierce, J. R., and Earhart, C. F. (1988) Biochemical analysis of spontaneous fepA mutants of *Escherichia coli*. *J. Gen. Microbiol. 134*, 1355−1364.
11. Dioumaev, A. K., Brown, L. S., Needleman, R., and Lanyi, J. K. (1999) Fourier transform infrared spectra of a late intermediate of the bacteriorhodopsin photocycle suggest transient protonation of Asp-212. *Biochemistry 38*, 10070−10078.
12. Dioumaev, A. K., Brown, L. S., Needleman, R., and Lanyi, J. K. (2001) Coupling of the reisomerization of the retinal, proton uptake, and reprotonation of Asp-96 in the N photointermediate of bacteriorhodopsin. *Biochemistry 40*, 11308−11317.
13. Dioumaev, A. K. (1997) Evaluation of intrinsic chemical kinetics and transient product spectra from time-resolved spectroscopic data. *Biophys. Chem. 67*, 1−25.
14. Dioumaev, A. K., Richter, H.-T., Brown, L. S., Tanio, M., Tuzi, S., Saitô, H., Kimura, Y., Needleman, R., and Lanyi, J. K. (1998) Existence of a proton-transfer chain in bacteriorhodopsin: participation of Glu-194 in the release of protons to the extracellular surface. *Biochemistry 37*, 2496−2506.
15. Shrager, R. I., and Hendler, R. W. (1982) Titration of individual components in a mixture with resolution of difference spectra, p*K*s, and redox transitions. *Anal. Chem. 54*, 1147−1152.
16. Brown, L. S., Dioumaev, A. K., Needleman, R., and Lanyi, J. K. (1998) Connectivity of the retinal Schiff base to Asp^{85} and Asp^{96} during the bacteriorhodopsin photocycle: the local-access model. *Biophys. J. 75*, 1455−1465.
17. Grzesiek, S., and Dencher, N. A. (1986) Time-course and stoichiometry of light-induced proton release and uptake during the photocycle of bacteriorhodopsin. *FEBS Lett. 208*, 337−342.
18. Braiman, M. S., Mogi, T., Marti, T., Stern, L. J., Khorana, H. G., and Rothschild, K. J. (1988) Vibrational spectroscopy of bacteriorhodopsin mutants: light-driven proton transport in-

volves protonation changes of aspartic acid residues 85, 96, and 212. *Biochemistry 27*, 8516−8520.
19. Braiman, M. S., Bousché, O., and Rothschild, K. J. (1991) Protein dynamics in the bacteriorhodopsin photocycle: submillisecond Fourier transform infrared spectra of the L, M, and N photointermediates. *Proc. Natl. Acad. Sci. U.S.A. 88*, 2388−2392.
20. Fahmy, K., Weidlich, O., Engelhard, M., Tittor, J., Oesterhelt, D., and Siebert, F. (1992) Identification of the proton acceptor of Schiff base deprotonation in bacteriorhodopsin: a Fourier transform infrared study of the mutant Asp85 → Glu in its natural lipid environment. *Photochem. Photobiol. 56*, 1073−1083.
21. Subramaniam, S., Marti, T., and Khorana, H. G. (1990) Protonation state of Asp (Glu)-85 regulates the purple-to-blue transition in bacteriorhodopsin mutants Arg-82 → Ala and Asp-85 → Glu: the blue form is inactive in proton translocation. *Proc. Natl. Acad. Sci. U.S.A. 87*, 1013−1017.
22. Otto, H., Marti, T., Holz, M., Mogi, T., Stern, L. J., Engel, F., Khorana, H. G., and Heyn, M. P. (1990) Substitution of amino acids Asp-85, Asp-212, and Arg-82 in bacteriorhodopsin affects the proton release phase of the pump and the p*K* of the Schiff base. *Proc. Natl. Acad. Sci. U.S.A. 87*, 1018−1022.
23. Oesterhelt, D., and Stoeckenius, W. (1971) Rhodopsin-like protein from the purple membrane of *Halobacterium halobium*. *Nat. New Biol. 233*, 149−152.
24. Lanyi, J. K., Tittor, J., Váró, G., Krippahl, G., and Oesterhelt, D. (1992) Influence of the size and protonation state of acidic residue 85 on the absorption spectrum and photoreaction of the bacteriorhodopsin chromophore. *Biochim. Biophys. Acta 1099*, 102−110.
25. Richter, H.-T., Needleman, R., and Lanyi, J. K. (1996) Perturbed interaction between residues 85 and 204 in Tyr-185 → Phe and Asp-85 → Glu bacteriorhodopsins. *Biophys. J. 71*, 3392−3398.
26. Balashov, S. P., Imasheva, E. S., Govindjee, R., and Ebrey, T. G. (1996) Titration of aspartate-85 in bacteriorhodopsin: what it says about chromophore isomerization and proton release. *Biophys. J. 70*, 473−481.
27. Butt, H.-J., Fendler, K., Bamberg, E., Tittor, J., and Oesterhelt, D. (1989) Aspartic acids 96 and 85 play a central role in the function of bacteriorhodopsin as a proton pump. *EMBO J. 8*, 1657−1663.
28. Sawatzki, J., Fischer, R., Scheer, H., and Siebert, F. (1990) Fourier transform Raman spectroscopy applied to photobiological systems. *Proc. Natl. Acad. Sci. U.S.A. 87*, 5903−5906.
29. Kakitani, H., Kakitani, T., Rodman, H., Honig, B., and Callender, R. H. (1983) Correlation of vibrational frequencies with absorption maxima in polyenes, rhodopsin, bacteriorhodopsin and retinal analogues. *J. Phys. Chem. 87*, 3620−3628.
30. Smith, S. O., Pardoen, J. A., Lugtenburg, J., and Mathies, R. A. (1987) Vibrational analysis of the 13-*cis*-retinal chromophore in dark-adapted bacteriorhodopsin. *J. Phys. Chem. 91*, 804−819.
31. Smith, S. O., Braiman, M. S., Myers, A. B., Pardoen, J. A., Courtin, J. M. L., Winkel, C., Lugtenburg, J., and Mathies, R. A. (1987) Vibrational analysis of the *all-trans* chromophore in light-adapted bacteriorhodopsin. *J. Am. Chem. Soc. 109*, 3108−3125.
32. Smith, S. O., Pardoen, J. A., Lugtenburg, J., Curry, B., and Mathies, R. A. (1983) Chromophore structure in bacteriorhodopsin's O_{640} photointermediate. *Biochemistry 22*, 6141−6148.
33. Kandori, H., Yamazaki, Y., Hatanaka, M., Needleman, R., Brown, L. S., Richter, H.-T., Lanyi, J. K., and Maeda, A. (1997) Time-resolved Fourier transform infrared study of structural changes in the last steps of the photocycles of Glu-204 and Leu-93 mutants of bacteriorhodopsin. *Biochemistry 36*, 5134−5141.
34. Zscherp, C., and Heberle, J. (1997) Infrared difference spectra of the intermediates L, M, N, and O of the bacteriorhodopsin photoreaction obtained by time-resolved attenuated total reflection spectroscopy. *J. Phys. Chem. B. 101*, 10542−10547.
35. Váró, G., and Lanyi, J. K. (1989) Photoreactions of bacteriorhodopsin at acid pH. *Biophys. J. 56*, 1143−1151.
36. Brown, L. S., Gat, Y., Sheves, M., Yamazaki, Y., Maeda, A., Needleman, R., and Lanyi, J. K. (1994) The retinal Schiff base-counterion complex of bacteriorhodopsin: changed geometry during the photocycle is a cause of proton transfer to aspartate 85. *Biochemistry 33*, 12001−12011.
37. Holz, M., Drachev, L. A., Mogi, T., Otto, H., Kaulen, A. D., Heyn, M. P., Skulachev, V. P., and Khorana, H. G. (1989) Replacement of aspartic acid-96 by asparagine in bacteriorhodopsin slows both the decay of the M intermediate and the associated proton movement. *Proc. Natl. Acad. Sci. U.S.A. 86*, 2167−2171.
38. Otto, H., Marti, T., Holz, M., Mogi, T., Lindau, M., Khorana, H. G., and Heyn, M. P. (1989) Aspartic acid-96 is the internal proton donor in the reprotonation of the Schiff base of bacteriorhodopsin. *Proc. Natl. Acad. Sci. U.S.A. 86*, 9228−9232.
39. Tittor, J., Soell, C., Oesterhelt, D., Butt, H.-J., and Bamberg, E. (1989) A defective proton pump, point-mutated bacteriorhodopsin Asp96 → Asn is fully reactivated by azide. *EMBO J. 8*, 3477−3482.
40. Cao, Y., Váró, G., Chang, M., Ni, B. F., Needleman, R., and Lanyi, J. K. (1991) Water is required for proton transfer from aspartate-96 to the bacteriorhodopsin Schiff base. *Biochemistry 30*, 10972−10979.
41. Drachev, L. A., Kaulen, A. D., and Komrakov, A. Y. (1992) Interrelations of M-intermediates in bacteriorhodopsin photocycle. *FEBS Lett. 313*, 248−250.
42. Delaney, J. K., Schmidt, P., Atkinson, G. H., and Subramaniam, S. (1997) Evidence for a long-lived 13-*cis*-containing intermediate in the photocycle of the Leu 93 → Ala bacteriorhodopsin mutant. *J. Phys. Chem. B. 101*, 5619−5621.
43. Zimányi, L., Váró, G., Chang, M., Ni, B., Needleman, R., and Lanyi, J. K. (1992) Pathways of proton release in the bacteriorhodopsin photocycle. *Biochemistry 31*, 8535−8543.
44. Cao, Y., Brown, L. S., Needleman, R., and Lanyi, J. K. (1993) Relationship of proton uptake on the cytoplasmic surface and reisomerization of the retinal in the bacteriorhodopsin photocycle: An attempt to understand the complex kinetics of the pH changes and the N and O intermediates. *Biochemistry 32*, 10239−10248.
45. Hessling, B., Souvignier, G., and Gerwert, K. (1993) A model-independent approach to assigning bacteriorhodopsin's intramolecular reactions to photocycle intermediates. *Biophys. J. 65*, 1929−1941.
46. Bergo, V., Spudich, E. N., Scott, K. L., Spudich, J. L., and Rothschild, K. J. (2000) FTIR analysis of the SII540 intermediate of sensory rhodopsin II: Asp73 is the Schiff base proton acceptor. *Biochemistry 39*, 2823−2830.
47. Rothschild, K. J., Zagaeski, M., and Cantore, W. A. (1981) Conformational changes of bacteriorhodopsin detected by Fourier transform infrared difference spectroscopy. *Biochim. Biophys. Res. Commun. 103*, 483−489.
48. Siebert, F., Mäntele, W., and Kreutz, W. (1982) Evidence for the protonation of two internal carboxylic groups during the photocycle of bacteriorhodopsin. *FEBS Lett. 141*, 82−87.
49. Maeda, A. (1995) Application of FTIR spectroscopy to the structural study on the function of bacteriorhodopsin. *Israel J. Chem. 35*, 387−400.
50. Althaus, T., Eisfeld, W., Lohrmann, R., and Stockburger, M. (1995) Application of Raman spectroscopy to retinal proteins. *Israel J. Chem. 35*, 227−251.
51. Pfefferlé, J.-M., Maeda, A., Sasaki, J., and Yoshizawa, T. (1991) Fourier transform infrared study of the N intermediate of bacteriorhodopsin. *Biochemistry 30*, 6548−6556.
52. Bousché, O., Braiman, M. S., He, Y. W., Marti, T., Khorana, H. G., and Rothschild, K. J. (1991) Vibrational spectroscopy of bacteriorhodopsin mutants. Evidence that Asp-96 deprotonates during the M → N transition. *J. Biol. Chem. 266*, 11063−11067.

53. Dioumaev, A. K. (2001) Infrared methods for monitoring the protonation state of carboxylic amino acids in the photocycle of bacteriorhodopsin. *Biochemistry (Moscow) 66*, 1269−1276.
54. Millero, F. J. (1979) Thermodynamics of the carbonate system in seawater. *Geochim. Cosmochim. Acta 43*, 1651−1661.
55. Weidlich, O., and Siebert, F. (1993) Time-resolved step scan FTIR investigations of the transition from KL to L in the bacteriorhodopsin photocycle. Identification of chromophore twists by assigning hydrogen out of plane (HOOP) bending vibrations. *Appl. Spectrosc. 47*, 1394−1400.
56. Sasaki, J., Maeda, A., Kato, C., and Hamaguchi, H. (1993) Time-resolved infrared spectral analysis of the KL-to-L conversion in the photocycle of bacteriorhodopsin. *Biochemistry 32*, 867−871.
57. Dioumaev, A. K., and Braiman, M. S. (1997) Two bathointermediates in the bacteriorhodopsin photocycle, distinguished by nanosecond time-resolved FTIR spectroscopy. *J. Phys. Chem. B. 101*, 1655−1662.

BI025563X